Quantifying inflow uncertainties in RANS simulations of urban pollutant dispersion

Accepted Manuscript

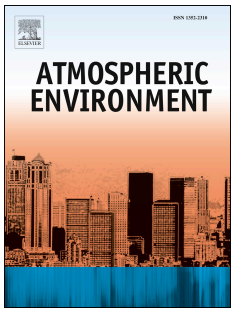

Quantifying inflow uncertainties in RANS simulations of urban pollutant dispersion

C. García-Sánchez, G. van Tendeloo, C. Gorlé

PII: S1352-2310(17)30257-1

DOI: 10.1016/j.atmosenv.2017.04.019

Reference: AEA 15286

To appear in: *Atmospheric Environment*

Received Date: 10 January 2017

Revised Date: 6 April 2017

Accepted Date: 10 April 2017

Please cite this article as: García-Sánchez, C., van Tendeloo, G., Gorlé, C., Quantifying inflow uncertainties in RANS simulations of urban pollutant dispersion, *Atmospheric Environment* (2017), doi: 10.1016/j.atmosenv.2017.04.019.

Quantifying inflow uncertainties in RANS simulations of urban pollutant dispersion

C. García-Sánchez[a,b,c,*], G. van Tendeloo[a], C. Gorlé[c]

[a] *EMAT, Department of Physics, University of Antwerp, Groenenborgerlaan 171, 2020 Antwerp, Belgium*
[b] *Von Karman Institute for Fluid Dynamics, Waterloosesteenweg 72, 1640 Sint-Genesius-Rode, Belgium*
[c] *Department of Civil and Environmental Engineering, Stanford University, 473 Via Ortega, Stanford, CA 94305, USA*

Abstract

Numerical simulations of flow and pollutant dispersion in urban environments have the potential to support design and policy decisions that could reduce the population's exposure to air pollution. Reynolds-averaged Navier-Stokes simulations are a common modeling technique for urban flow and dispersion, but several sources of uncertainty in the simulations can affect the accuracy of the results. The present study proposes a method to quantify the uncertainty related to variability in the inflow boundary conditions. The method is applied to predict flow and pollutant dispersion in downtown Oklahoma City and the results are compared to field measurements available from the Joint Urban 2003 measurement campaign. Three uncertain parameters that define the inflow profiles for velocity, turbulence kinetic energy and turbulence dissipation are defined: the velocity magnitude and direction, and the terrain roughness length. The uncertain parameter space is defined based on the available measurement data, and a non-intrusive propagation approach that employs 729 simulations is used to quantify the uncertainty in the simulation output. A variance based sensitivity analysis is performed to identify the most influential uncertain parameters, and it is shown that the predicted tracer concentrations are influenced by all three uncertain variables. Subsequently, we specify different probability distributions for the uncertain inflow

*Corresponding author
Email address: clara.garciasanchez@vki.ac.be (C. García-Sánchez)

variables based on the available measurement data and calculate the corresponding means and 95% confidence intervals for comparison with the field measurements at 35 locations in downtown Oklahoma City.

Keywords: urban flow, dispersion, Reynolds-Averaged Navier-Stokes, uncertainty quantification, Joint Urban 2003

1. Introduction

The latest World Health Organization (WHO) factsheet dedicated to ambient pollution shows that 92% of the world population lives in areas where the WHO air quality guidelines are not met [1]. The capability to provide accurate predictions of the dispersion of harmful pollutants in urban areas would enable supporting design and policy decisions to alleviate this problem. This motivates research into the use of computational fluid dynamics (CFD) to predict flow and dispersion phenomena in complex urban areas. A vast review of CFD studies of atmospheric boundary layer (ABL) flows in urban environments was recently published by Blocken [2]. The paper considered both Reynolds-averaged Navier-Stokes (RANS) [3, 4, 5, 6] and large-eddy simulations (LES) [7, 8, 9, 10, 11]. LES has the advantage of providing a more accurate representation of the turbulent flow features, since the larger, energy containing scales are resolved and only the small scales are modeled. Its main drawback is the significant amount of computational resources required, which is still limiting its use in complex engineering applications. As a result, more computationally affordable RANS simulations, which model the entire spectrum of turbulent scales, are commonly used in the wind engineering practice [12]. Several previous studies have performed steady and unsteady RANS simulations of dispersion of full-scale experimental campaigns [13, 14]. These studies focused on evaluating model performance by running a set of simulations with deterministic inflow conditions, and comparing their results with experimental data. Traditional performance metrics, such as fractional bias and normalized mean square error [15], were calculated, and varying degrees of success were reported, depending on the experimental period of time, the atmospheric stratification, and the intensity and variability of the inflow winds. These results indicate that the accuracy of RANS simulation results for urban flow and dispersion can be compromised by several sources of uncertainty.

Traditionally, a distinction is made between two types of uncertainty: the epistemic uncertainty, which is related to a lack of knowledge, and the aleatory uncertainty, which is intrinsic to the nature of the system and can not be reduced. In RANS simulations, the epistemic uncertainty largely originates from the turbulence modeling, and the development of methods to quantify this uncertainty is a relatively recent area of research [16, 17, 18, 19]. An important aleatory uncertainty is the definition of the inflow boundary conditions. These are influenced by the larger-scale atmospheric conditions and can therefore be highly variable [20, 21].

Previous research focused on quantifying the latter uncertainty in simulations of the flow in downtown Oklahoma City [22, 23]. In these studies we defined three uncertain parameters that define the inflow boundary condition: the wind speed and direction, and the ABL roughness length. To fully evaluate the capabilities of the approach we considered a test case for which field experiments are available for comparison to the UQ results. We selected the Joint Urban 2003 (JU2003) measurement campaign, which provides a full month of measurements in downtown Oklahoma City. We focused specifically on 30-minute time series of wind flow measurements at 13 locations in the downtown area using portable wind detectors (PWIDS). During the measurement campaign, the predominant wind direction was from the south, thus wind measurements from the south-most station were used to define probability density functions (pdfs) for the uncertain inflow parameters. A non-intrusive uncertainty quantification (UQ) approach based on 729 deterministic RANS simulations was used to propagate the inflow uncertainties to the simulation output. The resulting wind predictions for the mean and 95% confidence intervals were compared to the field measurements, showing that the 95% UQ confidence intervals encompassed all stations for the experimental mean velocity magnitude and 11 out of 13 stations for the experimental mean velocity direction.

The objective of the present research is to extend this study to quantify the inflow uncertainty in simulations of urban dispersion, and to include a more detailed analysis of the methodology and results. We focus on a different measurement period from the JU2003 campaign, considering one of the intensive observation periods that included a continuous tracer release to analyze dispersion. Wind and concentration measurements are compared to the UQ results using 35 portable and super portable wind detectors (PWIDS/SPWIDS), and 8 real time tracer analyzers located in the downtown area. As in [22, 23] we define three uncertain parameters to define the

inflow boundary conditions and we use a non-intrusive propagation method.

As a first step we perform a variance-based sensitivity analysis using the Sobol indices, which quantify the direct and combined contribution of the different uncertain inflow parameters to the variance of the quantities of interest. This type of analysis enables identifying the influential uncertain variables, and the conclusions could potentially reduce the number of evaluations needed for future UQ studies in urban environments. Subsequently we investigate the influence of the choice for the input pdfs by considering two different beta distributions fitted to the experimental data. The first represents the full variance of the experimental signal, and therefore represents all fluctuations in the measured signal as an inflow uncertainty. The second beta distribution represents a reduced variance, where the variance corresponding to the turbulence kinetic energy in the RANS model is removed from the measured signal, and only the remaining portion of the measured variance is considered an inflow uncertainty. Mean and 95% confidence intervals for the corresponding flow and tracer concentration fields are presented and compared to the available experimental data.

The remainder of this paper is organized in six sections. Section 2 summarizes the Joint Urban 2003 (JU2003) field measurements. Section 3 provides the details of the computational model, including the governing equations and their discretization, the boundary conditions applied, and the computational domain and mesh. Section 4 presents the uncertainty quantification (UQ) methodology, discussing the propagation algorithm, the calculation of the Sobol indices and the definition of the uncertain inflow parameters based on the experimental data. The sensitivity analysis and the comparison between field measurements and statistics for the flow and tracer concentration are presented in section 5. Conclusions and future research directions are formulated in section 6.

2. Experimental Campaign

The JU2003 experiments were performed over one full month during the summer of 2003 and provide day- and nighttime data for different boundary layer stratifications [24]. Previous modeling studies have used the database for evaluating models with differing degrees of complexity, and considering different scales. Chan and Leach [25] used it to evaluate and further develop the unsteady 3D finite element CFD code FEM3MP, while Neophytoua et al. [26] compared the measurements to results of different numerical ap-

proaches, ranging from rather simple to complex methods. In both studies the authors highlight the importance of the inflow boundary conditions to produce realistic urban flow predictions.

The specific data used for this study was obtained during one of the intensive observation periods (IOP9) with near-neutral flow conditions when sulfur hexafluoride (SF_6) was released in a continuous manner [27]. Specifically, the NOAA Air Resources Laboratory Field Research Division operated 8 mobile real-time analysers (ARLFRD) that provide concentration measurements. Wind measurements were performed by Dugway Proving Ground systems using 20 super portable wind detectors (SuperPWIDS) and 15 portable wind detectors (PWIDS), which are sonic and 3D sonic anemometers with sampling frequencies of 10Hz and 1Hz respectively. Figure 1 displays the location of the different measurement stations in downtown Oklahoma city, as well as the SF_6 source location. PWIDS 15, the south-most sensor, is used to define the uncertainty in the inflow variables as described in Section 4. All other sensor measurements will be used for validation of the model results.

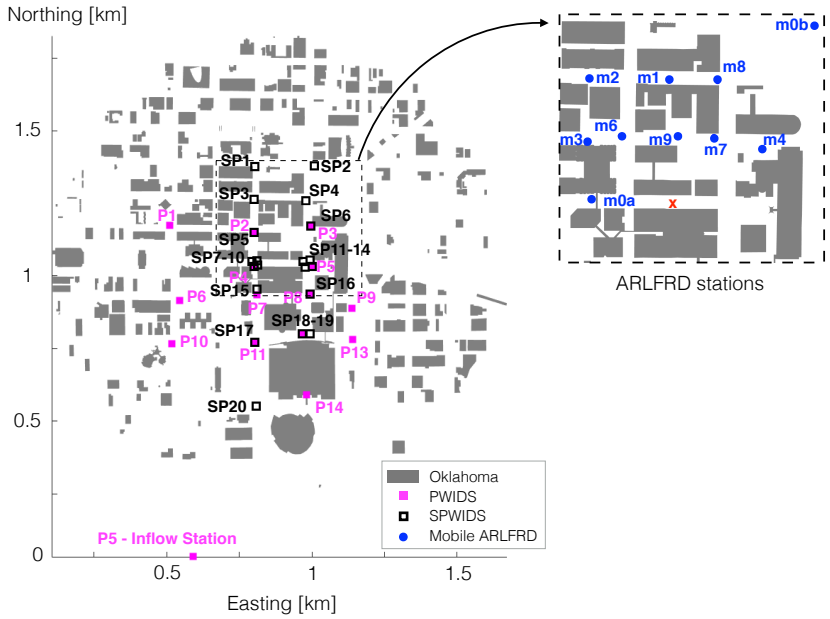

Figure 1: JU2003 measurement stations: portable wind detector (P, magenta squares), super portable wind detectors (SP, black squares) and tracer measurement mobile real time analysers (m, blue circles). SF_6 release location (red cross).

3. Computational model

3.1. Governing equations, discretization and solution method

The governing equations for the flow field are identical to those used in [22, 23]. The steady, incompressible Reynolds-averaged Navier-Stokes equations are used to solve the neutrally stratified ABL flow. Turbulence closure is obtained using the standard two equation k-ε turbulence model, which computes the Reynolds stresses using the linear eddy viscosity hypothesis [28].

To predict the concentration field, an additional transport equation for a passive scalar is solved [29]:

$$\overline{u_j}\frac{\partial \overline{C}}{\partial x_j} - \frac{\nu_t}{Sc_t}\frac{\partial^2 \overline{C}}{\partial x_j \partial x_j} = C_{source} \tag{1}$$

where $\overline{u_j}$ are the time-averaged velocity components, and $\overline{C}$ represents the time-averaged tracer concentration. Turbulent dispersion is represented using a standard gradient diffusion model, where the turbulent diffusion coefficient is defined as the ratio of the turbulent viscosity, ν_t, and the turbulent Schmidt number, Sc_t, which is fixed to a constant value of 0.7. The tracer is introduced continuously in the simulation in the cell corresponding to the location of the release of interest during IOP9 [24], as shown in Figure 1.

The equations were solved numerically using the open source set of libraries, OpenFOAM [30]. The flow equations are discretized using the finite-volume method, with second order upwind schemes for velocity, turbulence kinetic energy and turbulence dissipation. The simulations were run for 3000 iterations, which resulted in a converged solution with residuals below 1e-06 for all variables.

3.2. Computational domain and boundary conditions

The domain used to run the CFD simulations is presented in figure 2. The size of the domain was determined following the best practice guidelines from COST action 732 [31], which lead to a domain size of 4km by 3.9km in horizontal direction. The vertical domain height is 1.2 km, which equals $8H_{max}$, where $H_{max} = 150$m is the height of the tallest building in downtown Oklahoma City. All lateral boundaries are also located at a distance larger than $5H_{max}$ from the nearest building in order to avoid any unwanted effects from the boundary conditions on the flow solution. This design allows using

all lateral boundaries as either inlets or outlets, thereby efficiently enabling simulations for the different wind directions (70° to 120°) that occurred during IOP9. More specifically, a 90° wind direction, which corresponds to the wind coming from the south, would use the purple boundary from Figure 2 as an inflow, and the white boundary as an outflow. For inflow directions smaller than 90°, the blue boundary is an additional inflow, while the pink boundary is an additional outlet. The opposite would hold for inflow directions larger than 90°.

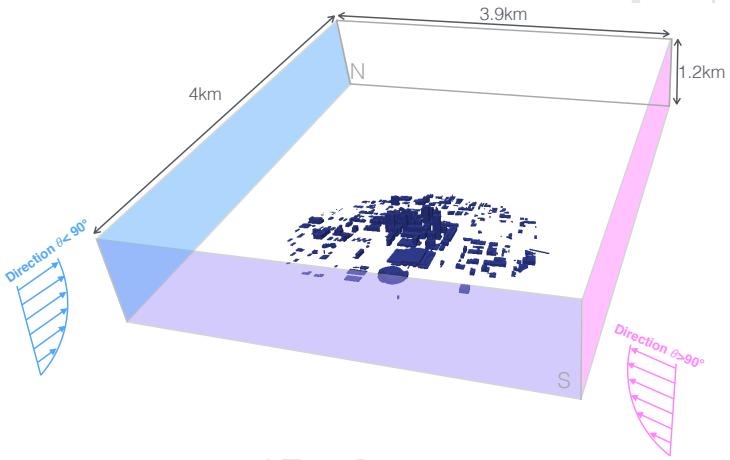

Figure 2: Computational Domain (N: north, S: south, South-North direction represents 90 degrees orientation).

At the outlets zero-gradient boundary conditions are imposed. On the inlets, the inflow boundary conditions represent a fully developed neutral surface layer [32], since the time-period selected from the experiments has near-neutral conditions. The surface layer profiles were used over the entire height of the domain. The influence of the profiles specified above 100m is expected to be negligible when considering quantities of interest at pedestrian level. The boundary conditions thus specify a logarithmic profile for velocity, a constant profile for turbulence kinetic energy, and a profile for epsilon that assumes equilibrium between turbulence kinetic energy production and dissipation:

$$U = \frac{u_*}{\kappa} ln \left(\frac{z + z_0}{z_0} \right) \tag{2}$$

$$k = \frac{u_*^2}{\sqrt{C_\mu}} \tag{3}$$

$$\varepsilon = \frac{u_*^3}{\kappa\,(z + z_0)} \tag{4}$$

U represents the mean velocity, κ the von Karman constant (0.41), k and ε the turbulence kinetic energy and dissipation rate, and C_μ is a turbulence model constant (0.09). The friction velocity is determined from the specified aerodynamic roughness, and the reference velocity, U_{inflow}, measured at 30m height by PWIDS 15 (figure 1).

At the top boundary a constant shear stress boundary condition is mimicked by specifying the velocity, turbulence kinetic energy and turbulence dissipation rate as the values given by the inlet profiles at the height of the top boundary. At wall boundaries a no-slip condition is imposed and wall functions are used to calculate the flow variables in the wall-adjacent cells. At the ground boundary an ABL wall function based on a constant ABL roughness length, z_0, is used. This wall function ensures that the neutral ABL inflow profiles for velocity, turbulence kinetic energy and turbulence dissipation rate are maintained downstream of the inlet [33, 34]. At the building walls a standard log law wall function for smooth surfaces is applied.

3.3. Computational mesh and grid dependency

The parallel mesh generator, SnappyHexMesh [30], is used to design the computational mesh. It consists of ∼7.4 million cells, the majority of which are hexahedral. The mesh is progressively refined to achieve the highest resolution in the downtown area where the tracer concentration measurements were performed. In this region, the vertical resolution ranges from 0.69 to 2m near the ground, while the near wall resolution on the building walls varies from 0.3 to 1.32m. Before performing the UQ study, a grid dependency study was performed by running simulations with a finer mesh consisting of 16.8 million cells.

The inflow parameters for the grid dependency study are specified to match the time-average of the measurement at PWIDS 15 during IOP9, being $U = 6.13ms^{-1}$, $z_0 = 0.29m$, and the wind direction $\theta = 97°$. Figure 3 presents a comparison of the velocity at the PWIDS stations between the time-averaged measurements and the RANS results from the two different meshes. For both cases we computed hit rates with the experimental data

[31]. The thresholds to produce a 'hit' for the velocity magnitude were 0.25 for the relative discrepancy, and 0.008 for the absolute values. For the velocity direction only an absolute threshold of 20° was used. We found no improvement when using the finer mesh compared to the nominal one. In addition, we calculated hit rates for the nominal mesh using the fine mesh results as the observation values, which produced a hit in more than 75 % of the measurement stations for both wind magnitude and direction. A similar analysis was performed for the predicted pollutant concentrations, which also showed no improvements when using the fine mesh compared to the nominal mesh.

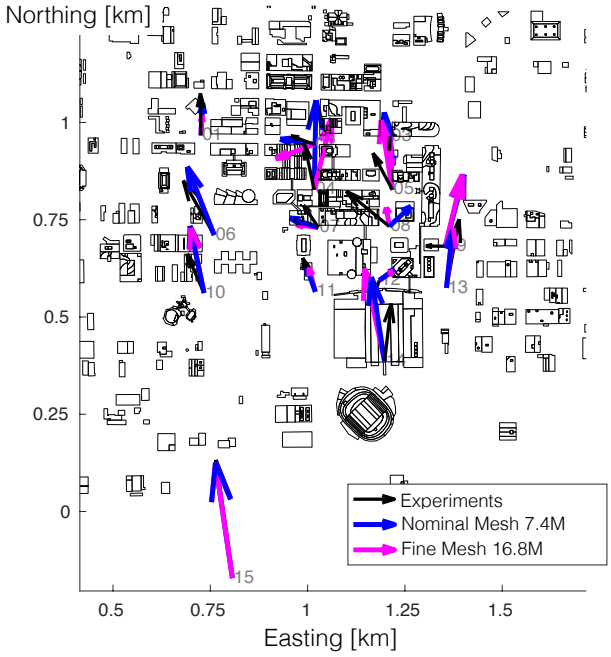

Figure 3: Comparison of the velocity vectors at the PWIDS stations: time-averaged measurements, RANS nominal mesh, and RANS fine mesh results.

Considering the relatively small changes in the predictions obtained with the nominal and fine mesh, and given the large number of simulations required for the UQ analysis, the nominal mesh has been employed for the remainder of the study.

4. Inflow Uncertainty Quantification Method

We characterize the uncertainty in the inflow boundary conditions specified by Eqs. 2-4 using three uncertain parameters: the wind direction, the wind magnitude at a reference height, and the upstream terrain roughness height z_0. The wind magnitude at a reference height is used to calculate the friction velocity u_*, thereby influencing the profiles for U, k and ϵ. In the following sections we first address the definition of probability distributions for the three uncertain parameters, and subsequently we summarize the UQ method, the calculation of the Sobol indices and the mean and 95% confidence intervals for the quantities of interest (QoI).

4.1. Characterization of uncertain inflow parameters

Characterizing the uncertain input parameters is an essential component of a UQ framework. For the initial sensitivity analysis we assumed uniform distributions for all three variables. The minima and maxima for the velocity magnitude and direction were obtained from the field measurements at PWIDS 15. This station is selected because it is the south-most measurement location and the wind direction during the measurements was predominantly from the south. The range for the aerodynamic roughness height was based on a roughness map of Oklahoma City available from [35].

For calculating the means and 95% confidence intervals, we propose a method to define more realistic, non-uniform, probability distributions. For the ABL roughness height, the available roughness map was digitally processed considering the area south of the city to build an approximate distribution for z_0, as presented in figure 4. Probability distributions for the velocity magnitude and direction are obtained from the experimental time series measured at PWIDS 15. Figure 4 presents the distributions from the 30 minute period of interest corresponding to the first continuous release during IOP9.

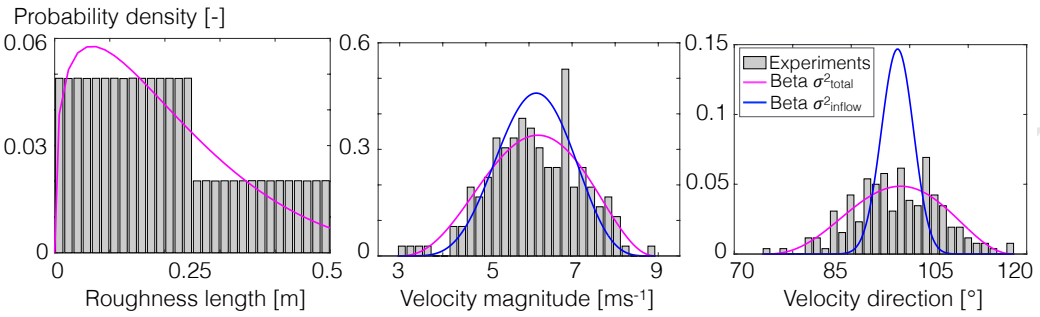

Figure 4: Probability density functions for the inflow uncertain parameters: roughness length, velocity magnitude and direction.

Figure 4 also depicts the beta probability density functions that were fitted to these distributions. These will be used to generate realizations from the spectral expansions for the quantities of interest, such that the mean and variance can be computed. For the velocity magnitude and direction, two different beta distributions will be considered. The coefficients for the first one, beta σ^2_{total}, were determined to match the mean and the variance of the experimentally measured time-series. The second one, beta σ^2_{inflow}, also matches the mean of the experiment but has a reduced variance. The rationale behind this second approach is that the turbulence model employed in the RANS simulations already accounts for part of the fluctuations in the measurements, hence this portion of the variance should not be represented by variability in the inflow conditions.

This 'variance reduction' methodology is based on the approach proposed by Vervecken et al. [36]. The conceptual idea is that the wind direction variance can be decoupled into two different contributions: a 'model' component that is represented by the turbulence model in the RANS simulation, and an 'external' or 'inflow' component related to the larger-scale variations in the atmospheric boundary layer, which are not represented by the RANS turbulence model. The fluctuating velocity is written as the sum of two different contributions: (1) the fluctuations represented by the RANS turbulence model, u'_m and v'_m ; and (2) the fluctuations induced by the 'external' or 'inflow' variability, u'_e and v'_e. It is assumed that the instantaneous spanwise velocity is much smaller than the instantaneous streamwise velocity ($v << u$), and that the fluctuations are small ($u' << u$). In addition the covariance of the modeled and external fluctuations is neglected. Using

these assumptions, the variance in the wind direction can be decomposed as follows:

$$\sigma_\theta^2 \approx \sigma_{\theta,inflow}^2 + \sigma_{\theta,m}^2, \tag{5}$$

where the modeled component can be approximated using

$$\sigma_{\theta,m}^2 \approx \frac{2/3k}{U^2}. \tag{6}$$

In previous works [23], we applied this relationship to define a beta pdf with reduced variance $\sigma_{\theta,inflow}^2$ for the wind direction. In the present work we extend this approach to also define a beta distribution with a reduced variance for the wind magnitude. Using the same assumptions as above, the total variance for the velocity magnitude can be written as:

$$\sigma_{\overline{U}}^2 \approx \sigma_{\overline{U},inflow}^2 + \sigma_{\overline{U},m}^2, \tag{7}$$

where the modeled contribution can be approximated as:

$$\sigma_{\overline{U},m}^2 \approx \frac{2}{3}k \tag{8}$$

The coefficients for the reduced variance beta distributions are therefore obtained by conserving the original mean from the PWIDS 15 measurement, and using the variances $\sigma_{\theta,inflow}^2$ and $\sigma_{\overline{U},inflow}^2$.

This variance reduction can be interpreted as a filtering operation on the original measurement data. If we assume the smaller scale fluctuations are represented by the turbulence model in the RANS simulations, we can find the cut-off frequency that accounts for the portion of the variance represented by $\sigma_{\theta,m}^2$ and $\sigma_{\overline{U},m}^2$. Figure 5 presents the normalized spectral energy density, indicating the cut-off frequency that separates the larger scale inflow variations from the smaller scale fluctuations represented by the turbulence model. Figure 6 presents the corresponding original and filtered signals for the velocity magnitude and direction at PWIDS 15. In section 5.2 we compare results for the means and 95% confidence intervals of the velocity and concentration field using both distributions to demonstrate the importance of the choice of the uncertain parameter space.

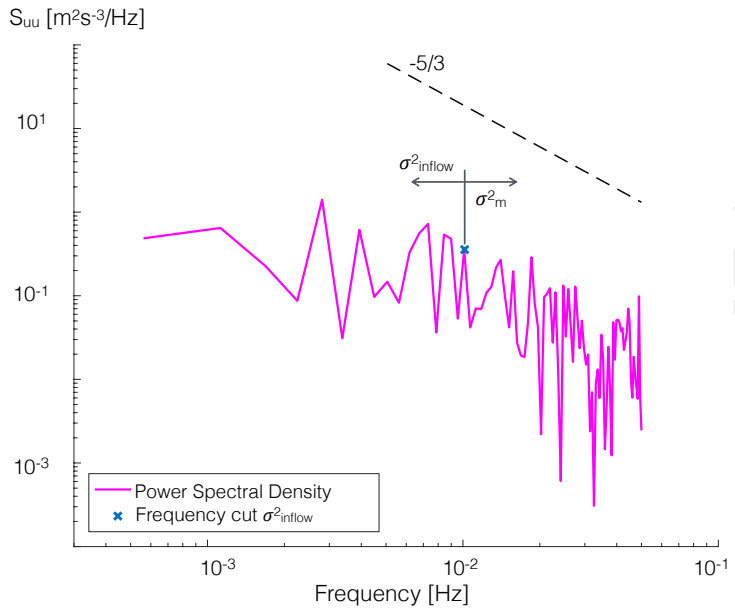

Figure 5: Normalized spectral energy density in function of frequency at PWIDS 15 station.

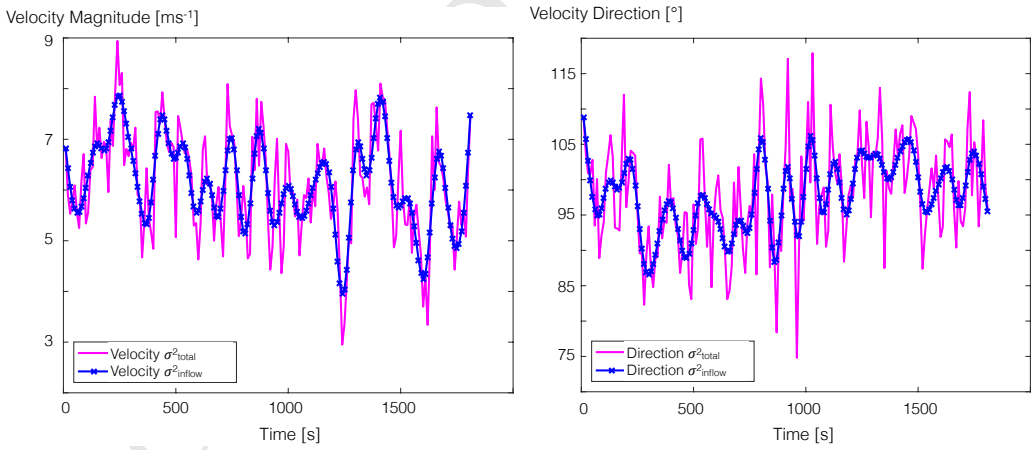

Figure 6: Original velocity magnitude and direction signals compared to the filtered signals considering uniquely inflow variance.

4.2. Propagation algorithm

The non-intrusive UQ code RAY developed at the Stanford UQ lab [37] was employed to propagate the inflow uncertainties to the output quanti-

ties of interest. The code requests user input regarding (1) the uncertain parameter space, i.e. minimum and maximum values for each uncertain parameter, (2) the quadrature method to be used, and (3) the maximum allowed number of simulations to perform the analysis. Using this information RAY determines the collocation points, i.e. the points in the 3D uncertain input parameter space for which simulations will be performed. Using the output of these simulations RAY constructs a spectral expansion and calculates statistics and probability distributions of the quantities of interest. The following sections subsequently describe the construction of the spectral expansion, the calculation of the Sobol indices, and the calculation of the statistics of the QoI in more detail [38].

4.2.1. Constructing the spectral expansion

The three uncertain inflow parameters, ξ_j are assumed to be mutually independent and uniform random variables. The n quantities of interest u^k are a function of ξ_j:

$$u^K = u^k\left(\xi_1, \xi_2, \xi_3\right) \qquad with \qquad k = 1, ..., n \tag{9}$$

Each variable ξ_j is defined on an interval Ξ_j, and the uncertain parameter space is characterized by the corresponding hypercube $\Xi = \Xi_1 \times \Xi_2 \times \Xi_3$. A probabilistic characterization of u^K can be obtained by formulating a spectral expansion:

$$u^K = \sum_{k=0}^{\infty} u_i^k \psi_i\left(\xi_1, \xi_2, \xi_3\right) \approx \sum_{i=0}^{P} u_i^k \psi_i\left(\xi_1, \xi_2, \xi_3\right), \tag{10}$$

where P is the order of truncation of the series and ψ_i are multivariate orthogonal polynomials. In the present study we employ Legendre polynomials and the maximum order of the polynomial terms is 4. The polynomial coefficients u_i^k are evaluated non-intrusively using Galerkin projection, with the integrals computed using Clenshaw-Curtis quadrature on an isotropic tensor grid:

$$u_i^k = \frac{\int\limits_{\Xi} u^k \psi_i d\xi_1 d\xi_2 d\xi 3}{\int\limits_{\Xi} \psi_i \psi_i d\xi_1 d\xi_2 d\xi 3} = \frac{\sum\limits_{l=0}^{N} u^k\left(\xi_1^l, \xi_2^l, \xi_3^l\right) \psi_i\left(\xi_1^l, \xi_2^l, \xi_3^l\right) w^l}{\sum\limits_{l=0}^{N} \psi_i\left(\xi_1^l, \xi_2^l, \xi_3^l\right) \psi_i\left(\xi_1^l, \xi_2^l, \xi_3^l\right) w^l}, \tag{11}$$

where $\left(\xi_1^l, \xi_2^l, \xi_3^l\right)$ is point l of the isotropic tensor grid (abscissa) and w^l are the integration weights.

4.2.2. Calculating the Sobol Indices

Direct and combined Sobol indices are commonly used to analyse the importance of the different uncertain parameters in a UQ analysis [39, 40]. The indices quantify the relative contribution of each uncertain variable to the variance of a QoI. The calculation of the Sobol indices is straightforward when the uncertain variables have probability density functions that are orthogonal to the polynomial basis. Hence, for this sensitivity analysis, we assume uniform distributions for all uncertain variables. The direct and combined Sobol indices can then be calculated as follows:

$$S_i = \frac{\sigma^2 \left[\mathbb{E}\left(u|\xi_i\right)\right]}{\sigma^2(u)} \tag{12}$$

$$S_{ij} = \frac{\sigma^2 \left[\mathbb{E}\left(u|\xi_i, \xi_j\right)\right]}{\sigma^2(u)} \tag{13}$$

The direct indices, S_i, provide a measure of the contribution of an isolated uncertain parameter, ξ_i, to the variance of the QoI. The combined indices, S_{ij}, quantify the contribution of a combination between different uncertain parameters ξ_i and ξ_j. The sum of all direct and combined Sobol indices is equal to 1. The expectations and variances required for this analysis are also easily computed by exploiting the orthogonality of the densities and the polynomial basis:

$$\mathbb{E}\left[u^K\right] = \int_{\Xi} u^k d\xi_1 d\xi_2 d\xi_3 \approx \sum_{i=0}^{P} u_i \Psi_i(\xi) \approx u_0 \tag{14}$$

while the variance would be calculated following:

$$\sigma^2\left[u^K\right] = \mathbb{E}\left[\left(u^K - \mathbb{E}\left[u^K\right]\right)^2\right] \approx \sum_{i=1}^{P} u_i^2 \left\langle \Psi_i(\xi) \right\rangle^2 \tag{15}$$

4.2.3. Calculating statistics for the output quantities of interest

For uncertain input variables with beta distributions as presented in figure 4 a different approach is required to compute statistics for the flow and concentration field. Once the spectral response surfaces for the quantities of interest are determined, probability density functions for u^K can be obtained by drawing realizations from the spectral representations according to the

beta distributions for the uncertain input variables. The mean and 95% confidence intervals are subsequently determined from these probability density functions. In the present analysis 10.000 realizations were used to calculate the statistics.

5. Results

In this section, we first present the sensitivity analysis. Subsequently, the analysis of the results focuses on the predicted mean and 95% confidence intervals (CI) for wind magnitude, direction and non-dimensional concentration.

5.1. Variance based sensitivity analysis

The analysis of the Sobol indices, which are calculated as explained in section 4, aims to investigate which of the uncertain input parameters contributes more to the variance of the quantities of interest. In the following the Sobol indices are presented together with the corresponding variance, since the analysis is particularly relevant in regions of the flow where the variance is larger. Figures 7, 8 and 9 therefore first present a contour plot for the variance of the quantity of interest under consideration in the upper left. Subsequently, from left to right and top to bottom, the other contour plots show the corresponding direct Sobol indices for the three uncertain variables (S_U, S_θ, and S_{z_0}), and two combined Sobol indices ($S_{U\theta}$ and $S_{\theta z_0}$).

5.1.1. Wind flows

Figure 7 presents the variance of the non dimensional velocity magnitude in downtown Oklahoma City and the corresponding direct and two of the combined Sobol indices. The variance contour plot for the predicted non-dimensional velocity magnitude shows that the variance becomes non negligible after the first row of buildings, and therefore the investigation of the Sobol indices is most relevant in those locations.

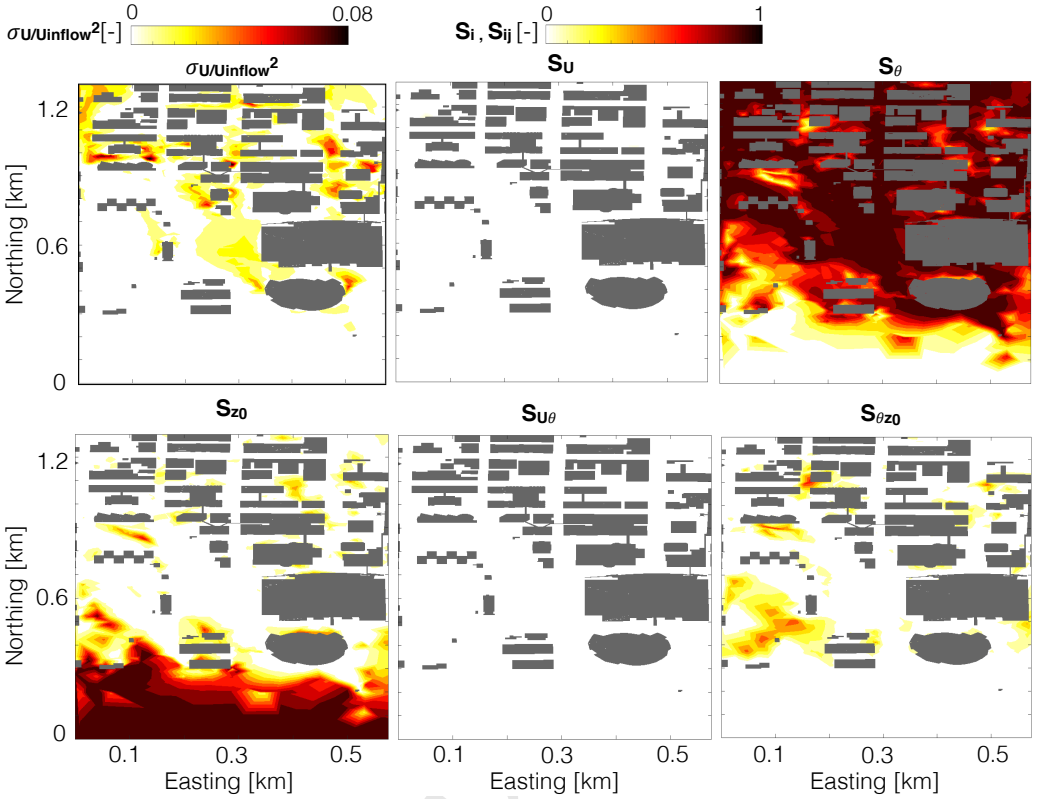

Figure 7: Sensitivity analysis for the prediction of the non-dimensional velocity magnitude U/U_{inflow} in downtown Oklahoma City: contour plots for the variance and the direct and combined Sobol indices.

The top center plot shows how the contribution of the uncertainty in the inflow velocity magnitude, quantified by S_U, is negligible. Downstream of the first row of buildings the most important contribution to the variance originates from uncertainty in the inflow wind direction as shown in the plot for S_θ. Upstream of the city the roughness length has the largest contribution to the variance, but the magnitude of the variance is small in this region. Some isolated locations in the flow field show additional sensitivity to the roughness length or to the combined effect between the inflow wind direction and the roughness length. These areas seem to correspond to larger recirculation zones. Combined sobol indices from the velocity magnitude with the other parameters shown negligible effects on the quantity of interest.

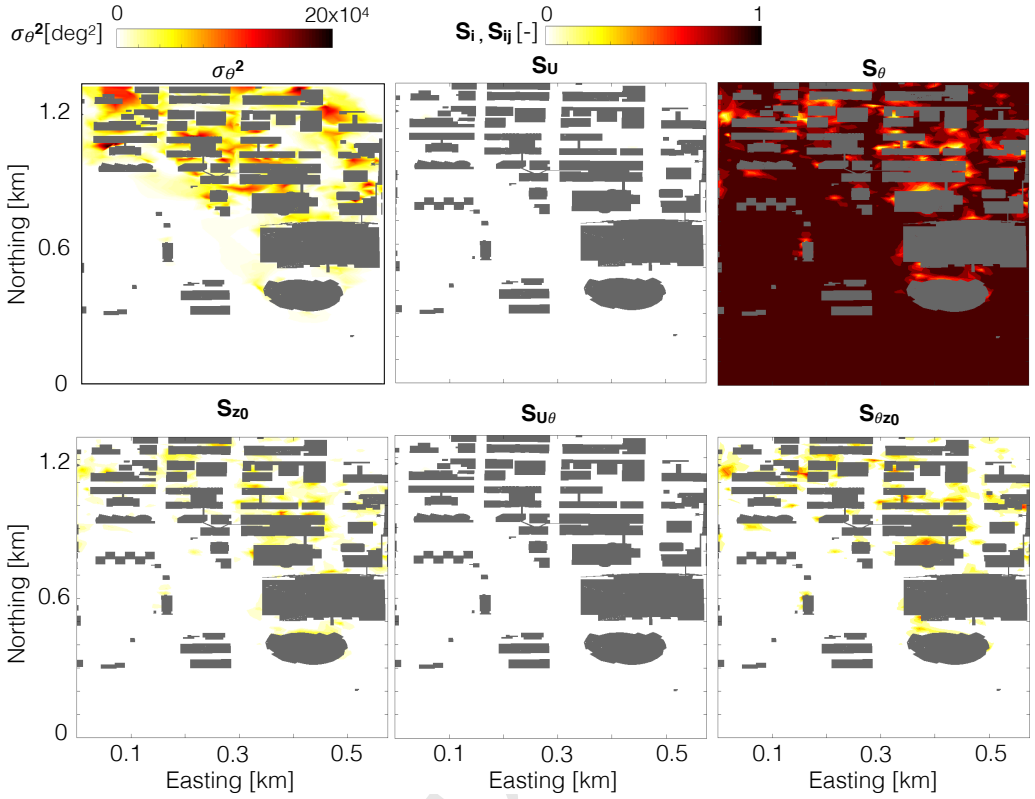

Figure 8: Sensitivity analysis for the prediction of the velocity direction θ in downtown Oklahoma City: contour plots for the variance and the direct and combined Sobol indices.

Figure 8 presents the variance of the flow direction in downtown Oklahoma City and the corresponding direct and combined Sobol indices. As for the velocity magnitude, the contour plot of the variance shows that the variance becomes non negligible after the first row of buildings. The contour plots of the Sobol indices clearly identify the uncertainty in the inflow velocity direction as the dominant factor.

5.1.2. Dispersion

Figure 9 depicts the variance of the non-dimensional tracer concentration and the corresponding Sobol indices. The non-dimensional concentration is defined as:

$$K = \frac{C^* H^2 U_{ref}}{Q_S} \tag{16}$$

where C^* represents the ratio between the local and the source concentrations, U_{ref} is the inflow velocity at 2m height, H is the average building height, set to 30m, and Q_S is the source flow rate.

The plots demonstrate that all three uncertain inflow parameters have a non-negligible effect. Near the source the variance is highest and the wind direction is shown to be the most influential parameter. As one would expect, it strongly determines the initial plume trajectory. Further downstream of the source, the sobol index for the wind direction decreases, and the inflow velocity magnitude and roughness length have a significant contribution to the variance. The combined Sobol indices for the wind magnitude and direction, and for the wind direction and roughness length also show non negligible contributions, indicating a complex interaction between the uncertain variables and the quantity of interest.

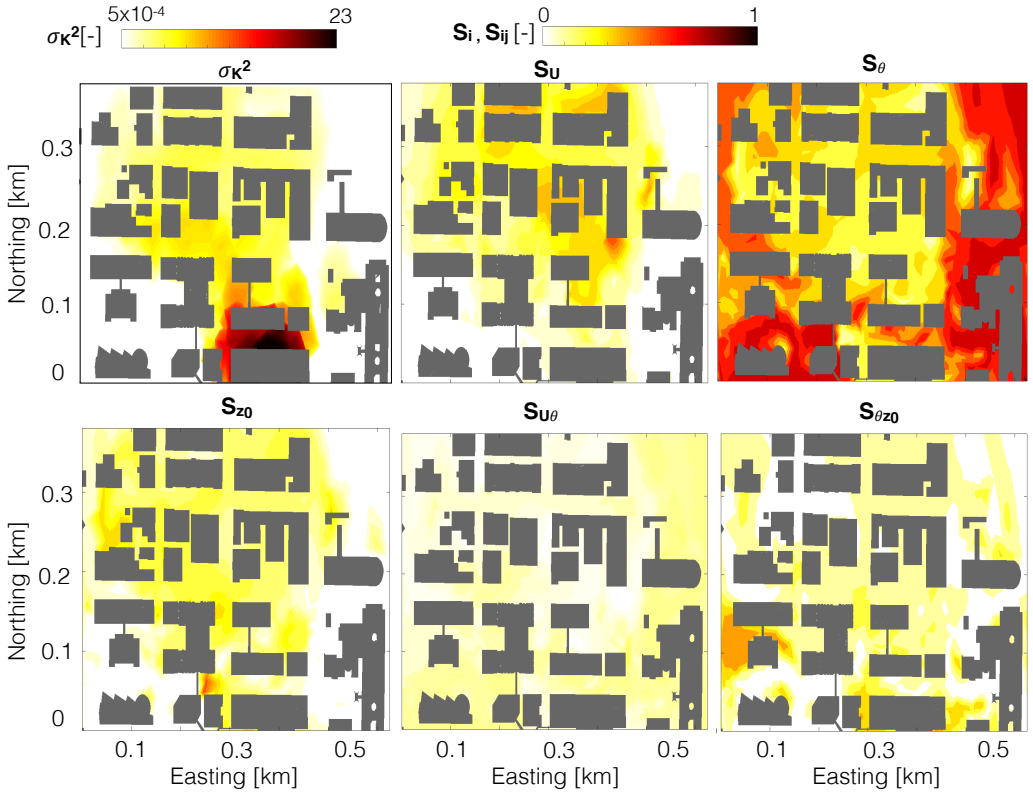

Figure 9: Sensitivity analysis for the prediction of the non-dimensional concentration K in downtown Oklahoma City: contour plots for the variance and the direct and combined Sobol indices.

5.2. Comparison of the predicted mean and 95% Confidence Intervals

The main objective of using the proposed UQ framework is to add confidence intervals to the simulation results that reflect the uncertainty in the solution related to variability in the inflow conditions. The confidence intervals should encompass the time-averaged field data measured during the period of interest, provided that other uncertainties are sufficiently small. The results for the wind field are presented by plotting the time-averaged experimental velocity vector at the measurement stations and compare that to the mean and 95% CI for the velocity predicted by the UQ study. The results for the concentration field are presented by plotting the mean with 95% CI bars for each measurement station.

5.2.1. Wind flow results

Figure 10 presents the results for the velocity field at the 13 PWIDS stations in the downtown area. The black arrows represent the velocity vectors from the field measurements, time-averaged over the experimental period of interest. The magenta and blue arrows show the mean from the UQ study, respectively obtained by assuming the previously presented beta distributions with the total and reduced variance for the inflow wind magnitude and direction (see Figure 4). The corresponding 95% confidence intervals for the predicted velocities are defined as the values where the cumulative density function is 0.025 and 0.975. They are represented in the plot by sectors of an annulus, where the 95% CI of the velocity magnitude is represented by the radii of the annulus, while the 95% CI for the wind direction is represented by the sector angle.

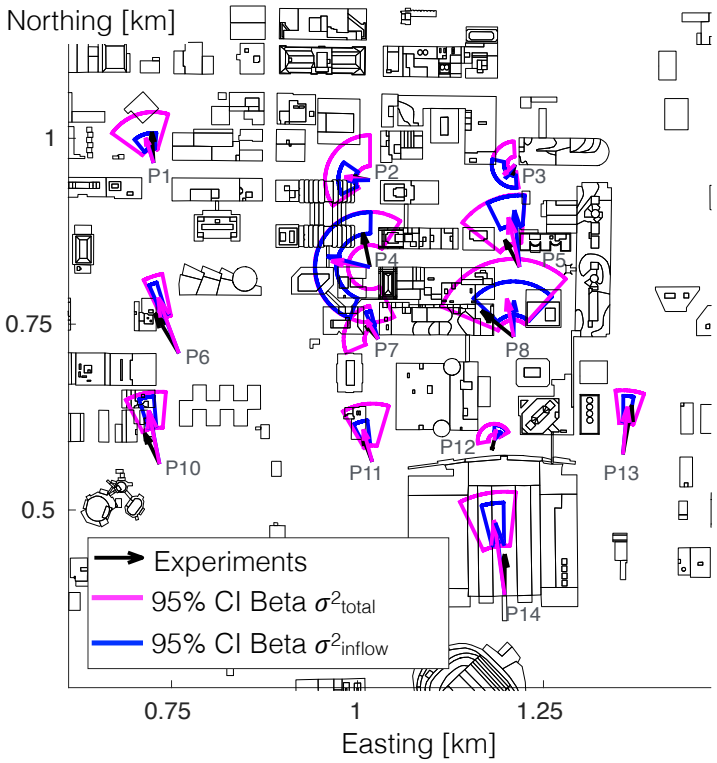

Figure 10: Comparison between experimental data and UQ study results for the wind prediction at the PWIDS stations.

The first observation from figure 10 is that the choice of the input pdfs for velocity magnitude and direction strongly affects the size of the 95% confidence intervals, while the prediction for the mean velocity only changes marginally. This is plausibly caused by the fact that the input pdfs differ in terms of the variance, but have the same mean value. When considering the inflow pdfs with the total variance, the 95% confidence interval from the UQ study encompasses the time-averaged measurement in 82% of the 35 (PWIDS and SPWIDS) measurement stations for the wind magnitude, and in 62% of the stations for wind direction. When considering the reduced inflow variance, these numbers reduce to 65% and 41% respectively.

The second observation from this plot is that the UQ study clearly differentiates between locations in the flow with a small versus large uncertainty caused by the inflow variability. For example PWIDS 6, 10, 11 and 13 all have small 95% CIs, while other stations in the downtown area, such as

PWIDS 3 and 4, present much larger uncertainty induced by the inflow variability. It is important to notice that this differentiation between the stations is consistent, i.e. it seems to be independent of the choice for the inflow pdfs.

5.2.2. Dispersion results

From the 10 SF_6 analysers for which the locations were shown in figure 1, only 8 were operational during the 30 minutes of interest. The mean and 95% CI for the non-dimensional concentration at these stations are presented in figure 11. The black crosses present the time-averaged measured value for K over the 30 minutes release, the magenta squares and confidence bars present the results from the UQ study using the total variance beta distributions as input, while the data plotted in blue corresponds to the inflow variance beta distribution.

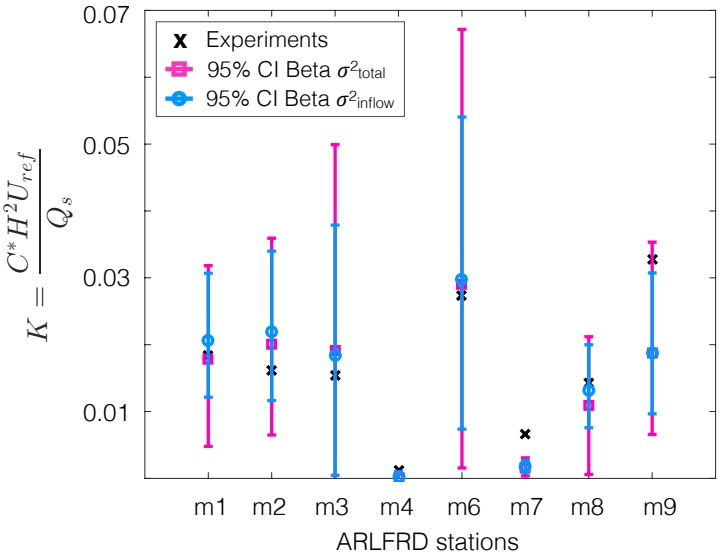

Figure 11: Comparison of the measurements during IOP9 with the uncertainty quantification study results for non dimensional concentration.

Similar as for the flow field, figure 11 shows that the choice of the input pdfs for velocity magnitude and direction strongly affects the size of the 95% confidence intervals, while the prediction for the mean concentration only changes marginally. Again, this is plausibly caused by the fact that the input pdfs differ in terms of the variance, but have the same mean value. In general, considering the mean from both UQ results, there is a slight over

prediction of the concentration in most of the stations. When using the beta distributions with the total variance, the experimental mean is encompassed by the 95% CI predicted by the UQ study in 75% of the stations. This number decreases to 63% when using the beta distributions with the reduced inflow variance.

The results for the concentration field also enable to differentiate between locations in the flow with smaller and larger uncertainty related to variability in the inflow conditions. For example, ARLFRD 1 and ARLFRD 6 exhibit larger uncertainty in the predicted pollutant concentration, while ARLFRD 7 has a smaller confidence interval.

5.2.3. Discussion on the definition of the uncertain parameter input distributions

The results for the flow and concentration field show a consistent behaviour in terms of the influence of the choice for the distributions for the uncertain input variables. The impact on the mean prediction is negligible, which can be explained by the fact that the means of the input pdfs are the same. The 95% confidence intervals increase with the variance of the input pdfs. As a result, the experimental mean falls within the 95% confidence interval in more locations when using the input pdfs that represent the total variance. Concluding that this approach is therefore better suited for quantifying inflow uncertainties in RANS simulations of urban flow and dispersion would however be premature. Instead, we argue that the input pdfs with the reduced variance are a more realistic representation of the uncertainty in the inflow conditions, and the resulting confidence intervals are a more accurate representation of the corresponding uncertainty in the solution. When these confidence intervals do not encompass the mean of the field experiment, this is an indication that additional uncertainties are likely to affect the solution. One specific example would be the uncertainty related to the turbulence model. Previous research [23] has addressed quantifying this uncertainty for the prediction of the flow field, and ongoing research is extending this approach to the prediction of the concentration field.

Lastly, the results presented for the velocity and concentration field show the potential of the approach to determine which areas within the city are more affected by uncertainties in the inflow boundary conditions. The resulting distinction between regions with larger and smaller uncertainties was shown to be independent of the choice of the input distributions. This indicates that the UQ approach can provide valuable information even if insuf-

ficient information is available to accurately characterize the input pdfs.

6. Conclusions

The boundary conditions for RANS simulations of urban pollutant dispersion are determined by the larger-scale atmospheric conditions, which can be highly variable. The present study investigates quantifying the resulting uncertainty in the prediction of urban wind and pollutant concentration. The proposed method defines three uncertain input parameters that specify the inflow boundary conditions: the wind velocity and direction, and the ABL roughness length. A non-intrusive uncertainty quantification (UQ) approach based on 729 deterministic RANS simulations is used to propagate the inflow uncertainties to the simulation output. The results of the UQ study are compared to field measurements from the Joint Urban 2003 (JU2003) measurement campaign.

An initial variance based sensitivity analysis was performed to investigate the influence of the different uncertain input parameters on the prediction of the QoI. The Sobol indices revealed that the prediction for the non-dimensional wind speed and wind direction is primarily influenced by uncertainty in the inflow wind direction, while the uncertainty in the inflow wind speed and roughness height are less influential parameters. When considering tracer concentrations all three uncertain variables were shown to contribute significantly to the variance in the QoI. This result points towards opportunities for dimension reduction when the objective is to calculate the flow field. When also considering pollutant dispersion, none of the uncertain variables can be ignored, but the required number of evaluations could potentially be reduced by using an anisotropic tensor grid [41].

The analysis of the results focused on comparing the prediction for the mean and 95% confidence intervals to the field measurement data. We investigated the influence of the choice for the input pdfs for the uncertain inflow velocity magnitude and direction by considering two different beta distributions. The first represents the full variance of the experimental signal measured at the most upstream location, and therefore represents all fluctuations in the measured signal as an inflow uncertainty. The second beta distribution represents a reduced variance, where the variance corresponding to the turbulence kinetic energy in the RANS model is removed from the measured signal, and only the remaining portion of the measured variance is considered an inflow uncertainty. When using the beta distributions with

the total variance, the predicted 95% confidence interval encompasses the time-averaged field measurement in 82% of the stations for wind magnitude, 62% for wind direction and 75% for the tracer concentration. These numbers respectively drop to 65%, 41%, and 63% when the beta distribution with the reduced inflow variance is used. Despite this decrease in the number of points where the predicted confidence intervals encompass the field measurements, we argue that the input pdfs with the reduced variance are a more realistic representation of the uncertainty in the inflow conditions. The fact that the corresponding confidence intervals do not encompass the mean of the field experiment, is an indication that additional uncertainties might be affecting the solution. One specific example would be the uncertainty related to the turbulence model, and ongoing research is focused on addressing this uncertainty.

In summary, the results demonstrate that there is considerable uncertainty in the prediction of urban flow and dispersion because of variability in the inflow conditions. It is important to note this is an aleatory uncertainty; it represents physical variability inherent to the system being analysed. It is not strictly due to a lack of knowledge and can therefore not be reduced. Additional experimental characterization might provide more conclusive evidence of the variability but cannot eliminate it completely and the aleatory uncertainty should therefore be characterized using probabilistic approaches. The definition of the input pdfs for the uncertain variables was shown to be crucial to obtain an accurate prediction for the 95% confidence interval. The variance-based sensitivity analysis enabled identifying the most relevant uncertain parameters, which will guide future research efforts regarding a more accurate definition of the input pdfs. However, the results also show that even in absence of sufficiently accurate information to define the input pdfs, the proposed UQ approach can provide valuable information regarding which areas in the urban canopy are more sensitive to the uncertain input parameters. This information can be used to guide design decisions, such as the implementation of additional geometrical features, that can reduce these sensitivities and therefore establish more predictable flow and dispersion patterns.

Acknowledgements

The first author's contribution to this work was supported by the doctoral (PhD) grant number 131423 for strategic basic research from the Agency for

Innovation by Science and Technology in Flanders (IWT). This work used the Extreme Science and Engineering Discovery Environment (XSEDE), which is supported by National Science Foundation grant number CTS160009 [42].

[1] World Health Organization, Ambient (outdoor) air quality and health (November 2016).
URL http://www.who.int/mediacentre/factsheets/fs313/en/

[2] Blocken, B., Computational fluid dynamics for urban physics: Importance, scales, possibilities, limitations and ten tips and tricks towards accurate and reliable simulations, Building and Environment 91 (2015) 219–245.

[3] Stathopoulos, T., Pedestrian level winds and outdoor human comfort, Journal of Wind Engineering and Industrial Aerodynamics 94 (11) (2006) 769–80.

[4] Tominaga, Y., Stathopoulos, T., Turbulent Schmidt numbers for CFD analysis with various types of flowfield, Atmospheric Environment 41 (37) (2007) 8091–9.

[5] Gorlé, C., van Beeck, J., Rambaud, P., Dispersion in the Wake of a Rectangular Building: Validation of Two Reynolds-Averaged Navier-Stokes Modeling Approaches, Boundary Layer Meteorology 137 (1) (2010) 115–133.

[6] Gousseau, P., Blocken, B., van Heijst, G.J.F., CFD simulation of pollutant dispersion around isolated buildings: On the role of convective and turbulent mass fluxes in the prediction accuracy, Journal of Hazardous Materials 194 (2011) 422–434.

[7] Moonen, P., Gromke, C., Dorer, V., Performance assessment of Large Eddy Simulation (LES) for modeling dispersion in an urban street canyon with tree planting, Atmospheric Environment 75 (2013) 66–76.

[8] Shi, R.F., Cui, G.X., Wang, Z.S., Xu, C.X., Zhang, Z.S., Large eddy simulation of wind field and plume dispersion in building array, Atmospheric Environment 42 (6) (2008) 1083–1097.

[9] Boppana, V.B.L., Xie, Z.-T., Castro, I.P., Large-eddy simulation of dispersion from surface sources in arrays of obstacles, Boundary Layer Meteorology 135 (3) (2010) 433–454.

[10] Xie, Z.-T., Hayden, P. and Wood, C.R., Large-eddy simulation of approaching-flow stratification on dispersion over arrays of buildings, Atmospheric Environment 71 (2013) 64–74.

[11] Muñoz-Esparza, D., Kosovic, B., van Beeck, J., Mirocha, J.D., A stochastic perturbation method to generate inflow turbulence in large-eddy simulation models: Application to neutrally stratified atmospheric boundary layers, Physics of Fluids 27 (2015) 035102.

[12] Tominaga, Y., Stathopoulos, T., CFD simulation of near-field pollutant dispersion in the urban environment: A review of current modeling techniques, Atmospheric Environment 79 (2013) 716–730.

[13] Hendricks, E.A., Diehl, S.R., Burrows, D.A., Keith, R., Evaluation of a fast-running urban dispersion modeling system using joint urban 2003 field data, Journal of Applied Meteorology and Climatology 46 (2007) 2165–2179.

[14] Kumar, P., Feiz, A.-A., Ngae, P., Kumar Singh, S., Issartel, J.-P., CFD simulation of short-range plume dispersion from a point release in an urban like environment, Atmospheric Environment 122 (2015) 645–656.

[15] Chang, J.C., Hanna, S.R., Air quality model performance evaluation, Meteorology and Atmospheric Physics 87 (1) (2004) 167–196.

[16] Emory, M., Larsson, J., Iaccarino, G., Modeling of structural uncertainties in Reynolds-averaged Navier-Stokes closures, Physics of Fluids 25 (11) (2013) 110822.

[17] Gorlé, C., Iaccarino, G., A framework for epistemic uncertainty quantification of turbulent scalar flux models for Reynolds-averaged Navier-Stokes simulations, Physics of Fluids 25 (2013) 055105.

[18] Gorlé, C., Larsson, J., Emory, G., Iaccarino, G., The deviation from parallel shear flow as an indicator of linear eddy-viscosity model inaccuracy, Physics of Fluids 26 (5) (2014) 051702.

[19] Xiao, H., Wu, J.-L., Wang, J.-X.,Sun, R., Roy, C.J., Quantifying and reducing model-form uncertainties in Reynolds-averaged Navier-Stokes simulations: A data-driven, physics-informed Bayesian approach, Journal of Computational Physics 324 (2016) 115–136.

[20] Schatzmann, M., Leitl, B., Issues with validation of urban flow and dispersion CFD models, Journal of Wind Engineering and Industrial Aerodynamics 99 (2011) 169–186.

[21] Rodriguez, L.M., Bieringer, P.E., Warner, T., Urban transport and dispersion model sensitivity to wind direction uncertainty and source location, Atmospheric Environment 64 (2013) 25–39.

[22] García-Sánchez, C., Philips, D.A., Gorlé, C., Quantifying inflow uncertainties for CFD simulations of the flow in downtown Oklahoma City, Building and Environment 78 (118-129).

[23] Gorlé, C., García-Sánchez, C., Iaccarino, G., Quantifying inflow and RANS turbulence model form uncertainties for wind engineering flows, Journal of Wind Engineering and Industrial Aerodynamics 144 (2015) 202–212.

[24] Allwine, K.J., Flaherty, J.E., Joint Urban 2003: Study Overview and Instrument Locations, PR 15967, PNNL (2006).

[25] Chan, S.T, Leach, M.J., A validation of FEM3MP with joint urban 2003 data, Journal of Applied Meteorology and Climatology 46 (2007) 2127–2146.

[26] Neophytoua, M., Gowardhan, A. , Brown, M., An inter-comparison of three urban wind models using Oklahoma city joint urban 2003 wind field measurements, Journal of Wind Engineering and Industrial Aerodynamics 99 (4) (2011) 357–368.

[27] Storwold, D., Meteorology division CSTE-DTC-DP-WD-ME-M, UT 84022-5000, Building 4034/Room 111 Dugway (2003).

[28] Wilcox, D.C., Turbulence Modeling for CFD, La Cañada: DCW Industries Inc., 1993.

[29] Pal Arya, S., Air pollution meteorology and dispersion, Oxford University Press, 1999.

[30] Greenshields, C.J., CFD Direct Ltd., Openfoam user guide, Tech. rep., OpenFOAM Foundation Ltd. (2011-2016).

[31] Franke, J., Best practide guideline for the CFD simulation of flows in the urban environment, COST Action 732, 2007.

[32] Richards, P.J., Hoxey, R.P., Appropriate boundary conditions for computational wind engineering models using the k-ε turbulence model, Journal of Wind Engineering and Industrial Aerodynamics 46-47 (1993) 145–153.

[33] Parente, A., Gorlé, C., van Beeck, J., Benocci, C., A comprehensive modelling approach for the neutral atmospheric boundary layer: consistent inflow conditions, wall function and turbulence model closure, Boundary Layer Meteorology 140 (3) (2011) 411–428.

[34] Blocken, B., Stathopoulos, T., Carmeliet, J., CFD simulation of the atmospheric boundary layer: wall function problems, Atmospheric Environment 41 (2) (2007) 238–252.

[35] Burian, S.J., Han, W.S., Brown, M.J., Morphological analyses using 3D building databases: Oklahoma City, Oklahoma, LANL Report LA-UR-05-1821 10, Los Alamos National Laboratory (2003).

[36] Vervecken, L., Camps, J., Meyers, J., Accounting for wind-direction fluctuations in reynolds-averaged simulation of near-range atmospheric dispersion, Atmospheric Environment 72 (2013) 142–150.

[37] Iaccarino, G., Introduction to uncertainty representation and propagation, AVT-193 short course on uncertainty quantification, Tech. rep., NATO Research and Technology Organization, Neuilly-sur-Seine (2011).

[38] Smith, R.C., Uncertainty Quantification: Theory, Implementation, and Applications, SIAM, Computational Science and Engineering, 2014.

[39] Sobol, I.M., Sensitivity analysis for non-linear athematical models, Mathematical Modeling and Computational Experiment 1 (1993) 407–414.

[40] Adams, B.M., Ebeida, M.S.,Eldred, M.S., Geraci, G., Jakeman, J.D., Maupin, K.A., Monschke, J.A., Swiler, L.P., Stephens, J.A., Vigil, D.M., Wildey, T.M., Bohnhoff, W.J., Dalbey, K.R., Eddy, J.P., Hooper, R.W., Hu, K.T., Hough, P.D., Ridgwayand, E.M., Rushdi, A., Dakota, a multilevel parallel object-oriented framework for design optimization, parameter estimation, uncertainty quantification, and sensitivity analysis: Version 6.3 theory manual, Tech. rep., SAND2014-4253 (2015).

[41] Paci, A., García-Sánchez, C., van Beeck, J., Gorlé, C., Uncertainty quantification for ABL flows, Project report VKI PR 2016-20, von Karman Institute for Fluid Dynamics (2015-2016).

[42] Towns, J., Cockerill, T., Dahan, M., Foster, I., Gaither, K., Grimshaw, A., Hazlewood, V., Lathrop, S., Lifka, D., Peterson, G.D., Roskies, R., Scott, J.R, Wilkins-Diehr, N., XSEDE: Accelerating Scientific Discovery, Computing in Science & Engineering 16 (2014) 62–74.

Highlights:

- The effect of inflow uncertainties in simulations of urban dispersion is quantified.
- The results are compared to the JU2003 experiments.
- Variance--based analysis shows wind direction is the dominant uncertain parameter.
- All uncertain parameters exhibit a non--negligible effect on urban dispersion.
- The results identify areas in the urban canopy more sensitive to inflow uncertainty.